Dalton Transactions

ROYAL SOCIETY OF CHEMISTRY

PAPER

View Article Online
View Journal | View Issue

Check for updates

Cite this: *Dalton Trans.*, 2024, **53**, 3756

A cross-metathesis approach for polymetallic [FeFe]-hydrogenase mimics†

Sergio Aguado, [a,c] Pablo García-Álvarez, [b,c] Javier A. Cabeza, [b,c] Luis Casarrubios *[a,c] and Miguel A. Sierra *[a,c]

Received 26th December 2023,
Accepted 22nd January 2024

DOI: 10.1039/d3dt04197b

rsc.li/dalton

A method has been developed for synthesizing [FeFe]-H_2ase mimics with diverse structures and properties, employing cross-metathesis of olefins. Vinylmetallocenes (**5** and **6**) and vinyl half-sandwich complexes (**10** and **11**) have been used as cross-metathesis partners with [FeFe]-H_2ase mimics (**4**, **8**, and **9**) bearing a double bond in the moiety attached to the ADT-bridge nitrogen. Electrochemical studies of these complexes, encompassing metallocene-type (**7a–b**, **12a–b**, and **13a–b**) as well as half-sandwich derivatives (**12c** and **13c–d**), have demonstrated that the introduction of a redox unit has a marginal impact on the reduction potential of these [FeFe]-H_2ase mimics. The application of this cross-metathesis approach has allowed the synthesis of [FeFe]-H_2ase mimics featuring an Ir(III) electrochemical antenna (**16–18**) as well as systems having an electron-donor-photosensitizer structure (ED-PS) (**23**). The electrocatalytic properties of these complexes have been elucidated through electrochemical studies.

Introduction

Hydrogenases are a class of metalloenzymes capable of catalyzing one of the simplest reactions in chemistry, namely the conversion of protons to molecular hydrogen.[1] These enzymes play a fundamental role in the energy metabolism of several microorganisms, as well as in the modulation of the redox potential of the microorganism cell.[2] Depending on the metabolic and energetic requisites of the cell, hydrogenase metalloenzymes can promote the evolution or the decomposition of molecular hydrogen. Additionally, these enzymes play a key role in the modulation of transmembrane proton gradients.[3] Reversible oxidation of molecular hydrogen occurs in the enzyme active metal-center.[4]

Depending on the nature of the metals present in this active centre, hydrogenases are classified into three different classes: [NiFe]- (**A**), [FeFe]- (**B**) and [Fe]-hydrogenases (**C**) (Fig. 1). The activity in the hydrogen evolution reaction (HER) depends on the enzyme type.[2] Thus, [FeFe]-hydrogenases ([FeFe]-H_2ases) are highly active in hydrogen production (up to 8000 μmol H_2 min^{-1} mg^{-1}),[5] while [NiFe]-hydrogenases efficiently catalyse the oxidation of hydrogen.[6] [Fe]-hydrogenases are present in some species of methanogenic archaea, catalysing the reduction of CO_2 to CH_4.[7] In this regard, the similarity of $[(\mu\text{-S})_2Fe_2(CO)_6]$ and the active centre of [FeFe]-H_2ases opened the possibility of using simplified models (mimics) of these enzymes to effect the HER. The use of these [FeFe]-H_2ase mimics has serious drawbacks with respect to the natural enzymes in the HER. Thus, different from the enzymes that can work at neutral pH, their mimics require lower pH values.[8] The electrocatalytic reduction of protons by [FeFe]-H_2ase mimics occurs at more negative potentials than that in natural enzymes with the subsequent overpotential cost.[9] Finally, the systems for H^+ and e^- transfer that are present in the enzymes are absent in the [FeFe]-H_2ase mimics. To solve these problems (knowing that the mimics present a higher tolerance to oxygen than the natural enzymes, which is one of

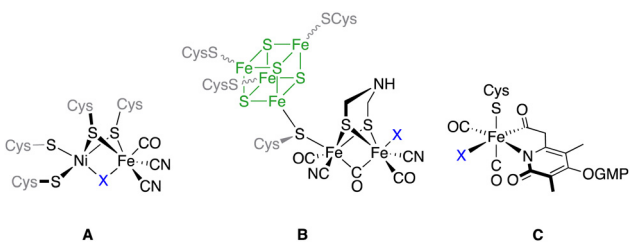

Fig. 1 The metal cores present in the three classes of hydrogenases. For [FeFe]-H_2ases, the Fe_4S_4 moiety has been drawn for clarity.

[a]*Departamento de Química Orgánica, Facultad de Ciencias Químicas, Universidad Complutense, 28040 Madrid, Spain. E-mail: sierraor@ucm.es, lcasarru@ucm.es*
[b]*Departamento de Química Orgánica e Inorgánica. Facultad de Química, Universidad de Oviedo, 33071 Oviedo, Spain*
[c]*Centro de Innovación en Química Avanzada (ORFEO-CINQA), Spain*

†Electronic supplementary information (ESI) available: Synthetic details, analytical data, and complementary XRD data. CCDC 2308698–2308700. For ESI and crystallographic data in CIF or other electronic format see DOI: https://doi.org/10.1039/d3dt04197b

the main shortcomings of these bio-catalysts) hundreds of [FeFe]-H_2ases have so far been designed and synthesised.[10]

The general approaches for the preparation of [FeFe]-H_2ases are limited to the direct reaction of $Fe(CO)_5$ or $Fe_3(CO)_{12}$ with sulphides and disulphides[11] to yield complexes **1** and to reactions of highly reduced species $[(\mu\text{-}S)_2Fe_2(CO)_6]^{2-}$ with formaldehyde imines (either as isolated species or as isolable trimers) or dichlorodimethyl amines, to form compounds **2**.[12] The [2 + 2]-cycloaddition of $[(\mu\text{-}S)_2Fe_2(CO)_6]$ to alkenes and alkynes affords complexes **3**. This approach is less efficient but it tolerates a large array of functional groups (Scheme 1).[13,14] The post-functionalization of simple [FeFe]-H_2ase mimics has been restricted to ligand interchange in the inner coordination sphere of the $[(\mu\text{-}S)_2Fe_2(CO)_6]$ derivative, or in other condensation reactions to attach these complexes to more complex molecular scaffolds.[15]

Recently, we approached the synthesis of some complex [FeFe]-H_2ase mimics by preparing the versatile reagent $[(\mu\text{-ADT})^{R}Fe_2(CO)_6]$ (R = *p*-$N_3C_6H_4$), and using this azide to introduce the [FeFe]-moiety into several substrates through a Cu-catalysed azide–alkyne cycloaddition.[16] In parallel, the use of easily available phosphites having three [FeFe]-moieties allowed the coordination of these polymetallic ligands to different square-planar and piano-stool complexes.[17] Moreover, the synthesis of heterometallic [FeFe]-mimics was carried out using tetranuclear complexes, in which the two [FeFe]-moieties were tethered by a bipyridine moiety suitable to complex different metals.[18] The electronic and electrocatalytic properties of these compounds were highly influenced by the presence of additional transition metal complexes either enhancing the electronic communication between the [FeFe] centers or inhibiting it, depending on the metal.

Pursuing the idea of developing new methodologies to access heterometallic [FeFe]-H_2ase mimics in an easy way and within the concept of precision chemistry, herein we report the preparation of several heteropolymetallic [FeFe]-H_2-ase mimics through a simple and efficient cross-metathesis (CM) reaction, also including a new triad having an [ED-PS-F_2S_2] structure with electron donor (ED) and photosensitizer (PS) moieties, as well as their electrochemical and electrocatalytic properties.

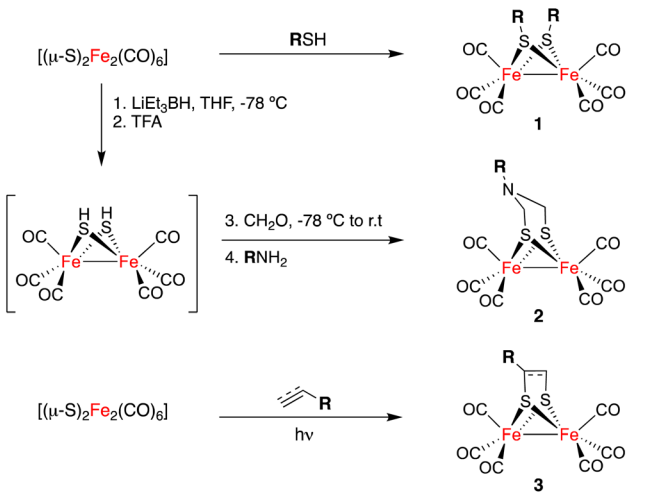

Scheme 1 The three main approaches for preparing [FeFe]-H_2ase mimics.

Results and discussion

The initial study was aimed to assess the viability (and optimization of the reaction conditions) of a cross-metathesis reaction (CM) between a vinylmetallocene and an [FeFe]-H_2ase mimic having a double bond attached to the nitrogen moiety of the adt-bridge. The reaction was studied using complex **4** [19] and vinylferrocene **5**.[20] The Grubbs GBI catalyst led to low yields of the desired product **7a**, requiring extended reaction times. The Hoveyda–Grubbs catalyst was more efficient but the main reaction products were homocoupling derivatives that were of little interest to fulfil our objectives. Finally, the use of the GBII catalyst led to the desired cross-metathesis product **7a** in an acceptable yield (52%, isolated), minimizing the formation of homocoupling reaction products. The optimum solvent for the cross-metathesis process using the GBII catalyst was dichloromethane. These reaction conditions were subsequently applied to the reaction of complex **4** with vinyl ruthenocene **6**, forming the cross-metathesis product **7b** in 42% yield (Scheme 2).

Complexes **7a** and **7b** are air-stable and were characterized by spectroscopic and spectrometric techniques. It is remarkable that both [FeFe]-H_2ase mimics were formed exclusively as their *E*-isomers. The signals of the olefinic protons for **7a** are clearly identified at 6.19 and 5.57 ppm (J = 15.6 Hz), while those for complex **7b** are observed at 6.07 and 5.57 ppm (J = 15.6 Hz). The structure of complex **7a** was unambiguously determined by X-ray diffraction (Fig. 2).

The generality of the process exemplified in Scheme 2 was proven by affecting the CM reactions of [FeFe]-hydrogenase mimics **8** and **9** with vinylmetallocenes **5** and **6** and half-sandwich complexes **10** and **11** (Scheme 3).[21,22] Metallocene derivatives containing the [FeFe]-H_2ase mimic moiety **12a–b** and **13a–b** were obtained in good yields and, consistently, exclu-

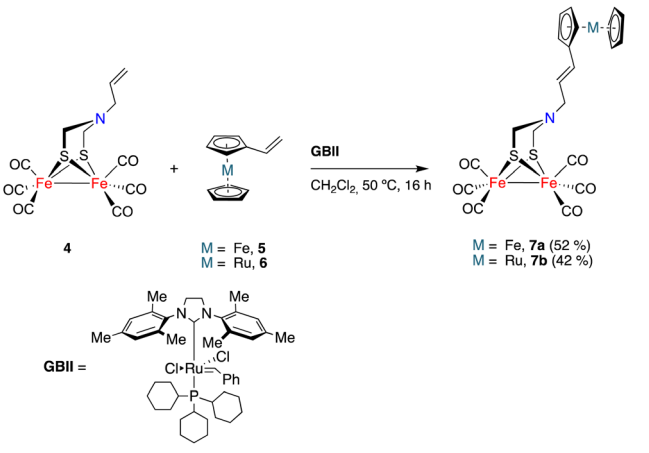

Scheme 2 Synthesis of [FeFe]-hydrogenase mimics **7a** and **7b**.

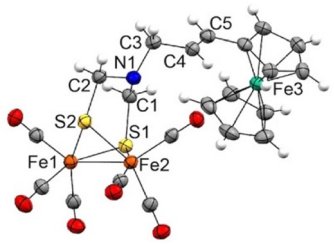

Fig. 2 The X-ray structure of polynuclear complex **7a** (30% displacement ellipsoids). Selected bond distances (Å): Fe1–Fe2 2.515(1), Fe1–S1 2.250(2), Fe1–S2 2.256(2), Fe2–S1 2.260(2), Fe2–S2 2.248(2), C1–N1 1.44 (1), C1–S1 1.829(8), C2–N1 1.433(9), C2–S2 1.845(7), C3–N1 1.485(9), C3–C4 1.492(10), C4–C5 1.32(1).

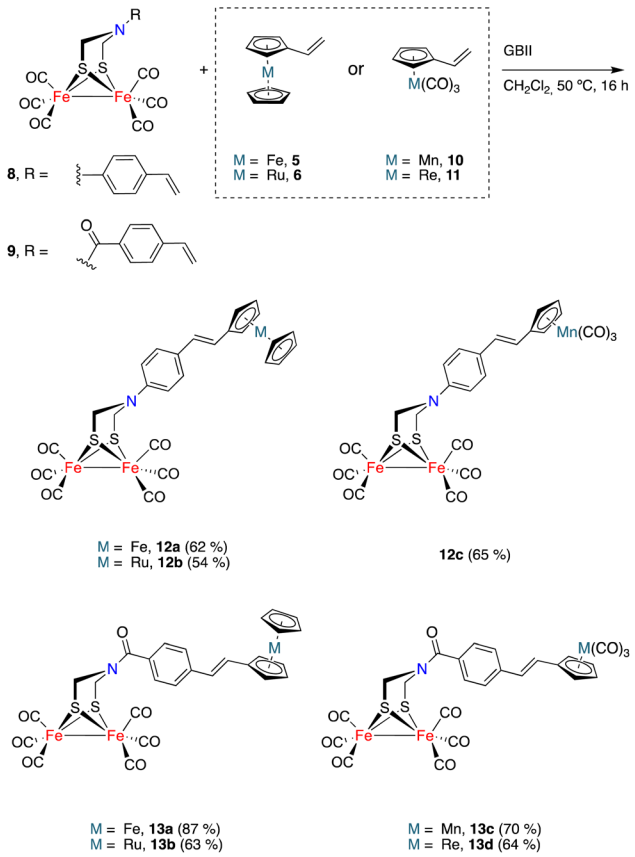

Scheme 3 Syntheses of [FeFe]-H_2ases bearing sandwich and half-sandwich moieties.

sively as their *E*-isomers. The analogous complexes **12c** and **13c–d**, having a half-sandwich moiety tethered to the [FeFe]-H_2ase mimic, were also obtained in good yields and again as their *E*-isomers. Yields for heterometallic mimics **13a** (87%) and **13b** (63%), derived from amides **9**, were higher than those of their amine analogues **12a** (62%) and **12b** (54%).

Complexes **12c** and **13c–d** show two signals in the M-CO region of their $^{13}C\{^1H\}$ NMR spectra. One, at around 207.0 ppm, is attributable to the six equivalent CO ligands of the [FeFe] moiety and the other is attributable to the $M(CO)_3$ moiety (224.1 ppm for Mn derivatives **12c** and **13c**, 193.9 ppm for the Re derivative **13d**). The X-ray structure of half-sandwich **12c** and metallocene **13b** confirm the proposed molecular structures and the geometry of the double bond (Fig. 3).

The possibility of applying the CM approach for the synthesis of [FeFe]-H_2ase mimics having octahedral Ir(III) moieties was next tested. [FeFe]-H_2ase mimics combining an octahedral photoactive moiety tethered to a $[(\mu\text{-ADT})Fe_2(CO)_6]$ fragment have been previously reported,[23] since the idea of the octahedral moiety acting as a photocatalyst to induce the electron transfer processes to the [FeFe] moiety is very attractive. Unfortunately, to date, efficient catalytic systems in the HER have not yet been achieved using this approach.[24,25]

Ir(III) complex **15** acting as a partner in the CM approach was prepared from $[Ir(\mu\text{-Cl})(C\text{^}N)_2]_2$ **14** and 2-(4-vinylphenyl) pyridine[26] in the presence of $Ag(CF_3SO_3)$ in boiling 2-ethoxyethanol. Complex **15** was obtained in 83% yield as an orange solid and as a single isomer, and is a thermodynamically favored[25] *fac* complex. Reactions of complex **15** with [FeFe]-mimics **4**, **8** and **9**, under the conditions reported above, gave heterotrimetallic complexes **16–18** in good yields (Scheme 4). Complexes **16–18** were air-stable and were characterized using spectroscopic techniques. Again, these complexes were obtained as *E*-isomers (^1H NMR $J_{CH=CH}$ = 15.8 Hz), showing the characteristic $^{13}C\{^1H\}$ NMR CO signals for the $[(\mu\text{-ADT})Fe_2(CO)_6]$ moiety in the 207–208 ppm range. These spectroscopic data together with the HRMS data support the heterotrimetallic structure proposed for complexes.

Finally, the CM approach for preparing [FeFe]-H_2ase mimics was also used to prepare the [ED-PS-Fe_2S_2] system **23** (Scheme 5), where ED is an electron donor moiety (ferrocene) and PS is a photoactive moiety (Ir(III) complex). The synthesis began with the preparation of dimeric Ir(III) complex **19** (having formyl groups) by the reaction of 2-(4-formylphenyl)

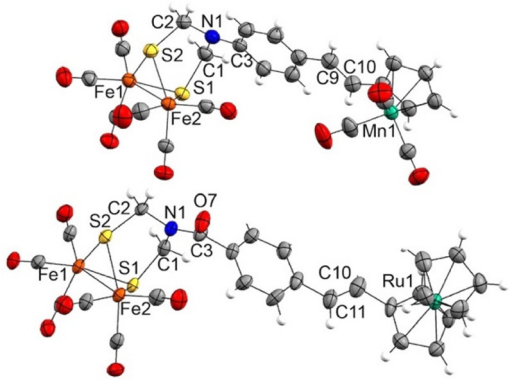

Fig. 3 X-ray structures of heterometallic complexes **12c** (top) and **13b** (bottom) (30% displacement ellipsoids). Selected bond distances (Å): **12c**: Fe1–Fe2 2.5070(8), Fe1–S1 2.2620(11), Fe1–S2 2.2580(11), Fe2–S1 2.2723(10), Fe2–S2 2.2533(11), C1–N1 1.428(6), C1–S1 1.870(4), C2–N1 1.420(6), C2–S2 1.871(5), C3–N1 1.397(6), C9–C10 1.311(8). **13b**: Fe1–Fe2 2.4944(18), Fe1–S1 2.249(2), Fe1–S2 2.257(3), Fe2–S1 2.271(2), Fe2–S2 2.268(2), C1–N1 1.427(12), C1–S1 1.850(10), C2–N1 1.452(10), C2–S2 1.846(9), C3–N1 1.352(12), C3–O7 1.240(12), C10–C11 1.249(19).

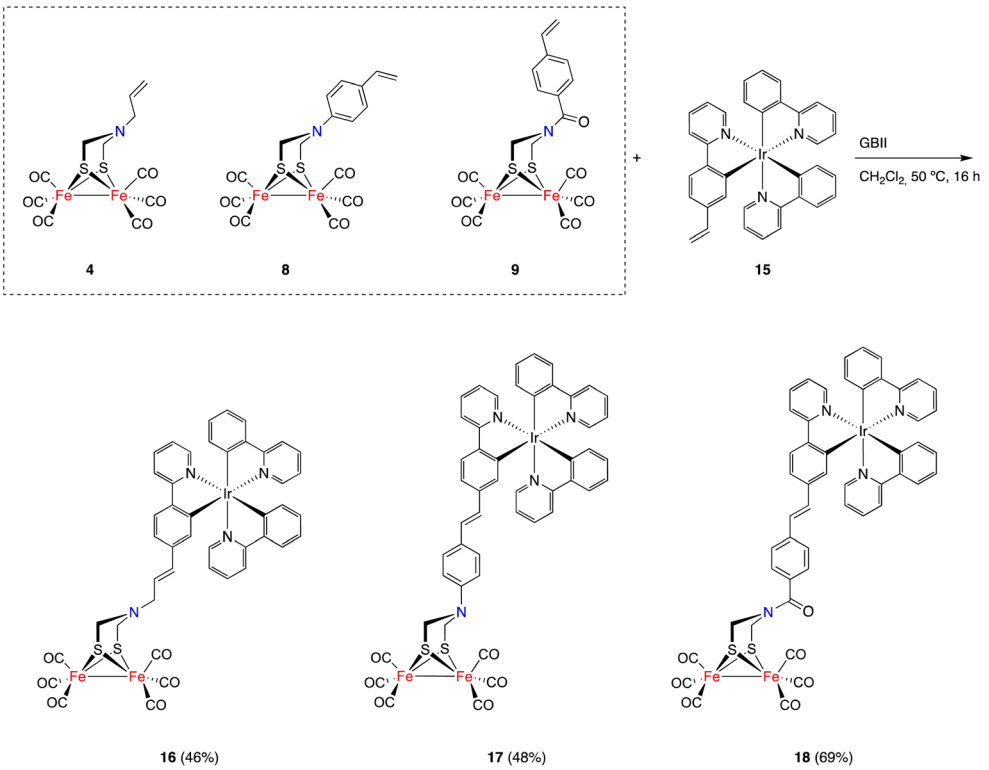

Scheme 4 The synthesis of heterometallic [FeFe]-H_2ase mimics.

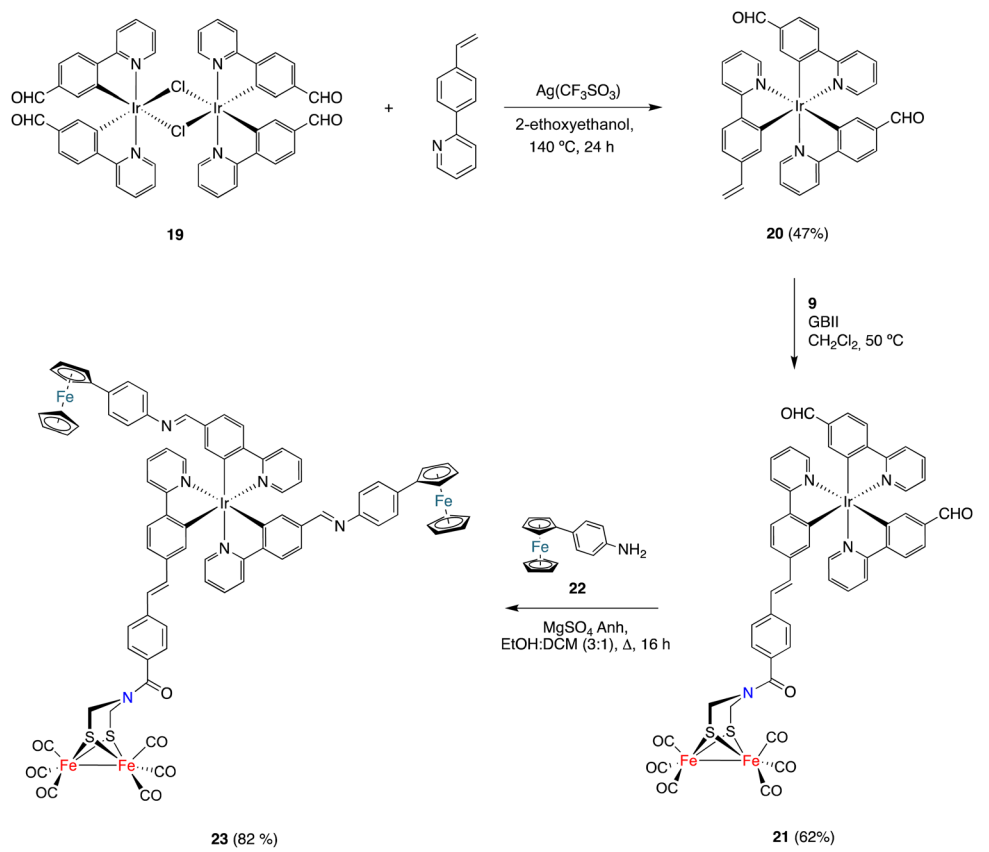

Scheme 5 The synthesis of the [ED-PS-Fe_2S_2] system **23**.

pyridine[27] with $IrCl_3.nH_2O$ in boiling 2-ethoxyethanol. This complex was obtained in 36% yield as a red solid. The dimeric structure of **19** was established using spectroscopic techniques. Its ^1H and $^{13}C\{^1H\}$ NMR spectra show a single set of signals, which pointed to the coexistence of a diastereomeric mixture of compounds in solution. The reaction of dimeric complex **19** with 2-(4-vinylphenyl)pyridine in boiling 2-ethoxyethanol in the presence of silver triflate formed complex **20**. The obtained solid was washed with EtOH and purified by silica gel chromatography (using DCM as the eluent) to obtain pure **20** as a red solid (47% yield). The structure of complex **20** was spectroscopically determined. The ^1H NMR spectrum shows the characteristic vinyl protons at 5.54 (dd, J_1 = 17.6, J_2 = 1,3 Hz) and 5.01 (dd, J = 10.8, J_2 = 1,3 Hz) ppm. The $^{13}C\{^1H\}$ NMR spectrum contains two signals, at 194.3 and 194.2 ppm, attributable to inequivalent aldehyde groups. This is consistent with a *fac*-disposition (thermodynamically favoured isomer).

Complex **20** was then reacted with alkene **9** under the CM conditions developed in this work. The CM product, namely complex **21**, was obtained in 62% yield. The HRMS and spectroscopic data were consistent with the proposed structure. Thus, a signal corresponding to the six CO groups of the [FeFe]-moiety appeared at 207.0 ppm in the $^{13}C\{^1H\}$ NMR spectrum, while the two signals appearing at 194.5 and 194.3 ppm correspond to the inequivalent formyl groups. Finally, the signal for the amide-CO group appeared at 162.9 ppm. The *E*-geometry was derived from the coupling of the protons attached to the double bond (J = 15.8 Hz).

To achieve the synthesis of the [ED-PS-Fe_2S_2] system **23**, complex **21** was condensed with *p*-aminophenyl ferrocene **19** [28] (2 equiv.) in a boiling solution of 3 : 1 EtOH/Cl_2CH_2. The desired complex was isolated as a red solid in 82% yield. Its structure was established using spectroscopic and HRMS techniques. Again, significant signals were observed for the two inequivalent imine protons at 8.29 and 8.23 ppm in the ^1H NMR spectrum and a sharp signal at 207.0 ppm was observed in the $^{13}C\{^1H\}$ NMR spectrum, supporting the integrity of the [(μ-ADT)$Fe_2(CO)_6$] moiety in the imine formation reaction.

Electrochemistry

Complexes **7a–b**, **12a–c** and **13a–d** show a quasireversible reduction wave in the range of −1.70 V to −1.60 V (*vs.* $Fc^{+/0}$). This wave is attributable to the [Fe^IFe^I] to [Fe^IFe^0] reduction (Fig. S-1† and Table 1).[29] Complexes **4**, **8** and **9** have been included for comparison. The small displacement in the reduction wave of complex **13a** with respect to **7a** agrees with the reported scarce influence of the substituent R attached to the nitrogen of the ADT-bridge of [(μ-ADT)$N^RFe_2(CO)_6$] complexes in their reduction potential.[30]

All complexes show a second irreversible reduction wave at −2.10 V (*vs.* $Fc^{+/0}$), attributable to the reduction of [Fe^0Fe^I] to [Fe^0Fe^0], and a quasireversible oxidation wave at around 0.50 V, attributable to the [Fe^IFe^I] to [Fe^IFe^{II}] oxidation.[29] Additionally, complexes **4a**, **12a** and **13a** show the oxidation waves characteristic of the ferrocene moiety at 0.0 V (*vs.* $Fc^{+/0}$), while ruthenocene derivatives **4b**, **12b** and **13b** show the quasireversible oxidation wave at around 0.20 V (*vs.* $Fc^{+/0}$), corresponding to the Ru(II) to Ru(III) oxidation.

Table 1 Electrochemical data (first reduction). Potentials in V *vs.* $Fc^{+/0}$

Complex	E_{pc1}	E_{pa1}	$E_{(1)}$
4	−1.76	−1.65 (0.11)	−1.70
7a	−1.74	−1.64 (0.10)	−1.70
7b	−1.74	−1.64 (0.10)	−1.69
8	−1.70	−1.62 (0.08)	−1.66
12a	−1.69	−1.62 (0.07)	−1.65
12b	−1.69	−1.62 (0.07)	−1.66
12c	−1.69	−1.62 (0.07)	−1.65
9	−1.64	−1.57 (0.07)	−1.61
13a	−1.64	−1.55 (0.09)	−1.60
13b	−1.64	−1.59 (0.05)	−1.62
13c	−1.64	−1.58 (0.06)	−1.61
13d	−1.64	−1.58 (0.06)	−1.61

The electrocatalytic behavior of complexes **7**, **12** and **13** in the presence of mild (AcOH, pK_a^{MeCN} = 22.3[31]) and strong (CF_3COOH, pK_a^{MeCN} = 12.6[32]) acids was next studied. Fig. 4 compiles the results of both experiments. The electrochemistry in the presence of AcOH was the standard for related [(μ-ADT)$N^RFe_2(CO)_6$] complexes.[33] The current intensity for the first wave is independent of the amount of AcOH, while a strong increase in the current intensity was observed in the second wave (above 2.0 V). This behaviour is compatible with two successive reduction processes resulting in the HER.

Complexes **7**, **12** and **13** behave differently in the presence of TFA. Now the first reduction wave in the range of −1.60 to −1.70 V (*vs.* $Fc^{+/0}$) experiences a strong electrocatalytic response (Fig. S-3†). Moreover, this wave splits into two waves upon increasing the concentration of the acid, which is consistent with the reduction of the protonated species.

The different electrocatalytic responses were evaluated through the increase of the current intensity with the acid concentration of the first reduction process (i_{cat}) with respect to the basal current intensity of the same process in the absence the acid (i_p) (Fig. 4). Similarly, plotting of i_{cat}/i_p *vs.* [H^+] allowed

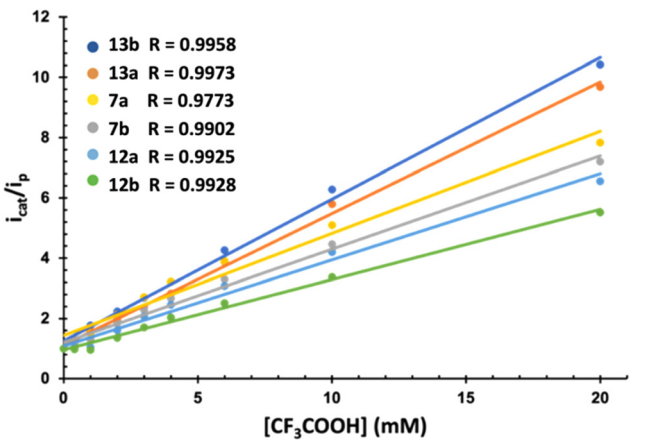

Fig. 4 Representation of i_{cat}/i_p for complexes **7**, **12** and **13** *vs.* TFA.

the calculation of the TOF for the reduction of H^+ (Table 2).[34] In all cases, the response increases linearly (Fig. 4), showing different sensibilities to the increase of $[H^+]$. Amide derivatives **13b** and **13a** showed a stronger electrocatalytic response.

Table 2 compiles the overpotentials (η) and the TOFs for the corresponding processes of all complexes. Amide derivatives **13d** and **13b** show higher TOFs. These values are 200% higher than that of **12a**, which clearly demonstrates the strong influence that the substituent in the ADT-bridge of [(μ-ADT)$N^RFe_2(CO)_6$] exerts on the kinetics (TOF) of these processes. These results may be explained by the fact that protonating the amide nitrogen of **13d** and **13b** is more difficult than protonating the amine moiety of complexes **7a–b** and **12a–c**. This difficulty may direct the protonation directly to the Fe nucleus or may trigger the proton transfer from the more acidic protonated amide to the Fe-nucleus.

The electrochemistry of [FeFe]-H_2ase mimics having octahedral Ir(III) moieties was next studied. Firstly, we registered the electrochemistry of complex **15**. Fig. 5 shows a reversible oxidation wave at 0.33 V (Ir^{III} to Ir^{IV}) (*vs.* $Fc^{+/0}$) and two reduction waves at −2.69 and −2.92 V (*vs.* $Fc^{+/0}$), attributable to both types of ppy ligands (ppy = 2-phenylpyridine).

Complexes **16–18** show a quasireversible reduction wave between −1.48 and −1.57 V (*vs.* $Fc^{+/0}$) (Fig. 6 and Table 3) that are attributable to the $[Fe^IFe^I]$ to $[Fe^IFe^0]$ reduction. Comparing with the reference voltammogram shown in Fig. 5, the additional reduction processes at around −1.98 and −2.09 V (*vs.* $Fc^{+/0}$) are attributable to the $[Fe^IFe^I]$ to $[Fe^0Fe^0]$ reduction. Reduction of the Ir(III) moiety was not seen in the window used. The oxidation waves of these compounds appeared in the range expected for the oxidation of Ir(III) to Ir(IV) moieties (0.33 V *vs.* $Fc^{0/+}$).[35] The main difference between complexes **15** and **16–18** in their oxidation waves is the irreversibility of the Ir(III) to Ir(IV) process observed for complex **16**, while complex **18** maintains the reversibility of the oxidation wave. Obviously, this behaviour should be related to the linker that connects the Ir and the FeFe centers, which is efficient in the case of the amide linker (probably due to its iminol tautomer), but it fails in the case of the enamine linker.

Table 2 Electrochemical data for complexes **7**, **12** and **13**. Potentials in V *vs.* $Fc^{+/0}$

Complex	$E_{Catalytic}$ [a] (V)	η [b] (V)	TOF [c] (s^{-1})
7a	−1.74	0.85	12.1
7b	−1.67	0.78	10.2
12a	−1.65	0.76	6.0
12b	−1.64	0.75	9.9
12c	−1.69	0.80	8.9
13a	−1.64	0.75	18.2
13b	−1.65	0.76	21.4
13c	−1.66	0.77	16.6
13d	−1.64	0.75	20.8

[a] Data obtained from Fig. S-3.† [b] Overpotential (η) calculated using $E^\circ_{HA} = -0.89$ V.[10] [c] TOF calculated with 20 mM TFA.

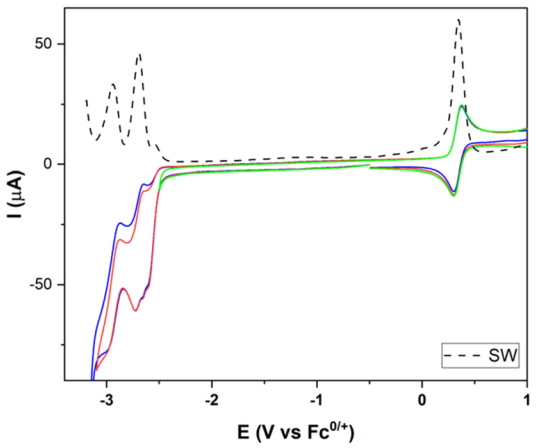

Fig. 5 CVs and SW of complex **15** in 10^{-3} M MeCN solutions containing $[^nBu_4N]PF_6$ 10^{-1} M as the supporting electrolyte (25 °C), Pt as the counter electrode, vitreum carbon as the working electrode; potentials in V *vs.* Fc^+/Fc; scan rate: 100 mV s^{-1}.

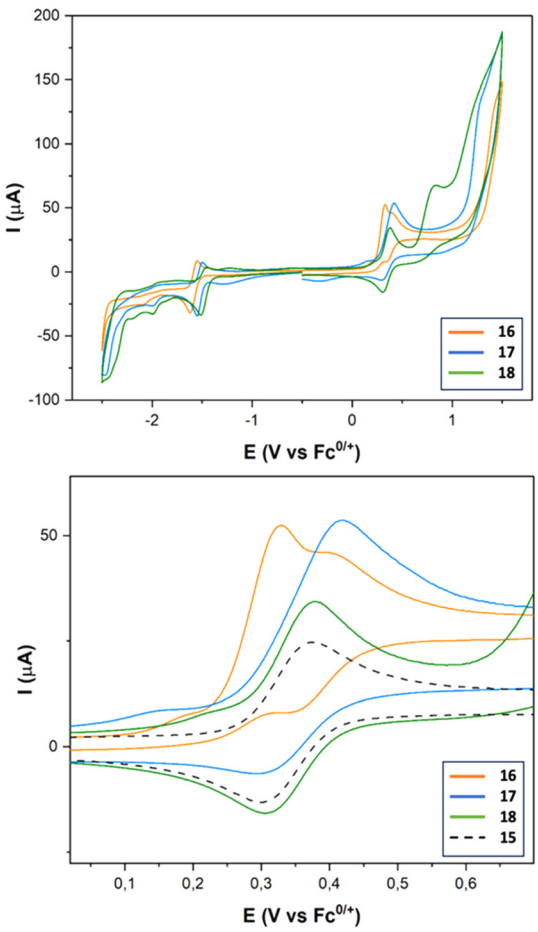

Fig. 6 CVs of complexes **16–18** (top) and expansion of the Ir^{III} to Ir^{IV} oxidation wave for **16–18** *vs.* **15** (bottom), obtained from 10^{-3} M solutions in MeCN containing $[^nBu_4N]PF_6$ 10^{-1} M as the supporting electrolyte, recorded at 25 °C. Counter-electrode: Pt; working electrode: vitreous carbon; potentials given in V *vs.* Fc^+/Fc; scan rate: 100 mV s^{-1}.

Table 3 Electrochemical data for **16–18**. Potentials in V *vs.* $Fc^{+/0}$

	$E_{(1)}$	E_{cat}	η^a	$TOF_{(10\ equiv.)}$	$TOF_{(20\ equiv.)}$
16	−1.57	−1.60	−0.71	2.5	2.5
17	−1.52	−1.61	−0.72	11.5	11.5
18	−1.48	−1.63	−0.74	17.4	53.3

Data obtained from Fig. S-4.† [a] Overpotential (η) calculated using $E^{\circ}_{HA} = -0.89$ V.[10]

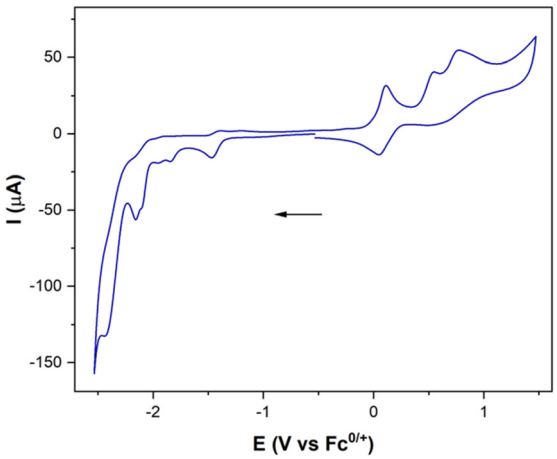

Fig. 7 CV of complex **23**, obtained from 10^{-3} M solutions in MeCN containing $[^nBu_4N]PF_6$ 10^{-1} M as the supporting electrolyte, recorded at 25 °C. Counter-electrode: Pt; working electrode: vitreous carbon; potentials given in V *vs.* Fc^+/Fc; scan rate: 100 mV s^{-1}.

To assess the electrocatalytic properties, an electrochemical study was conducted in the presence of a strong acid (CF_3COOH, pK_a^{MeCN} = 12.6[32]). Complexes **16–18** exhibit a strong electrocatalytic response (see Fig. S-4†). TOF values were calculated using the same H^+ source. Complex **18** shows the highest value (200-fold with respect to that of **16**), like the series of complexes **7**, **12** and **13**. Evidently, the nature of the linker between the new metal and the FeFe centres determine the electrocatalytic activity of these complexes.

To complete the study, the electrochemical response of the [ED-PS-Fe_2S_2] system **23** was measured. The [Fe^IFe^I] to [Fe^IFe^0] reduction appears at −1.43 V (*vs.* $Fc^{+/0}$) and the [Fe^IFe^0] to [Fe^0Fe^0] reduction process appears at −1.95 V (*vs.* $Fc^{+/0}$). The successive oxidation processes at 0.08 V (reversible) and 0.53 V (*vs.* $Fc^{+/0}$) correspond to the ferrocene and iridium moieties (Fig. 7).

Conclusions

The cross-metathesis coupling of [FeFe]-H_2ase mimics having double bond-containing moieties attached to the nitrogen of the adt bridge with vinyl metallocenes and half-sandwich and octahedral Ir(III) complexes having a vinyl functionality enables the syntheses of diverse heteropolymetallic [FeFe]-H_2ase mimics in an easy and efficient way. The new complexes have an *E*-stereochemistry across the formed double bond.

Electrochemical studies on both metallocenes (**7a–b**, **12a–b**, and **13a–b**) and half-sandwich derivatives (**12c** and **13c–d**) have revealed that the placement of a redox unit has only a minimum impact on the reduction potentials of these [FeFe]-H_2ase mimics.

The application of this cross-metathesis approach also allowed the synthesis of complexes having an electron-donor-photosensitizer structure (ED-PS) (**23**) bonded to the nitrogen of the adt-bridge. The electrocatalytic properties of these complexes have been elucidated. We observed a clear increase in the electrocatalytic response (a 200-fold increase in the TOF values for the HER) upon replacing an amine group with an amide group. This significant enhancement is attributed to the potential of the iminol tautomer to act as an efficient proton transfer group. In summary, an easy, efficient and versatile synthetic approach for [FeFe]-H_2ase mimics has been developed.

Author contributions

M. A. S. and L. C. designed and supervised the experimental work. S. A. performed the synthetic and characterisation experiments. J. A. C. and P. G.-A. determined the X-ray structures. All authors contributed to writing the manuscript.

Conflicts of interest

There are no conflicts to declare.

Acknowledgements

Support for this work under grants PID2019-108429RB-I00 (to M. A. S), PID2019-104652GB-I00 (to J. A. C and P. G-A) and RED2022-134287-T (ORFEO-CINQA network), from the MCIN (Spain), is gratefully acknowledged. Technical support provided by Servicios Científico-Técnicos de la Universidad de Oviedo is also acknowledged.

References

1 (*a*) P. M. Vignais and B. Billoud, Occurrence, Classification, and Biological Function of Hydrogenases: An Overview, *Chem. Rev.*, 2007, **107**, 4206–4272; (*b*) B. L. Greene, Progress and Opportunities in Photochemical Enzymology of Oxidoreductases, *ACS Catal.*, 2021, **11**, 14635–14650.

2 (*a*) J. C. Fontecilla-Camps, P. Amara, C. Cavazza, Y. Nicolet and A. Volbeda, Structure-function relationships of anaerobic gas-processing metalloenzymes, *Nature*, 2009, **460**, 814–822; (*b*) S. T. Stripp, B. R. Duffus, V. Fourmond, C. Léger, S. Leimkühler, S. Hirota, Y. Hu, A. Jasniewski, H. Ogata and M. W. Ribbe, Second and Outer Coordination Sphere Effects

in Nitrogenase, Hydrogenase, Formate Dehydrogenase, and CO Dehydrogenase, *Chem. Rev.*, 2022, **122**, 11900–11973.

3 P. M. Vignais, B. Billoud and J. Meyer, Classification and phylogeny of hydrogenases1, *FEMS Microbiol. Rev.*, 2001, **25**, 455–501.

4 W. Lubitz, H. Ogata, O. Rüdiger and E. Reijerse, Hydrogenases, *Chem. Rev.*, 2014, **114**, 4081–4148.

5 S. T. Stripp and T. Happe, How algae produce hydrogen—news from the photosynthetic hydrogenase, *Dalton Trans.*, 2009, 9960–9969.

6 H. Ogata, K. Nishikawa and W. Lubitz, Hydrogens detected by subatomic resolution protein crystallography in a [NiFe] hydrogenase, *Nature*, 2015, **520**, 571–574.

7 B. Schwörer, V. M. Fernandez, C. Zirngibl and R. K. Thauer, H_2-forming N5,N10-methylenetetrahydromethanopterin dehydrogenase from Methanobacterium thermoautotrophicum. Studies of the catalytic mechanism of H_2 formation using hydrogen isotopes, *Eur. J. Biochem.*, 1993, **212**, 255–261.

8 J. T. Kleinhaus, F. Wittkamp, S. Yadav, D. Siegmund and U.-P. Apfel, [FeFe]-Hydrogenases: maturation and reactivity of enzymatic systems and overview of biomimetic models, *Chem. Soc. Rev.*, 2021, **50**, 1668–1784.

9 D. Schilter, J. M. Camara, M. T. Huynh, S. Hammes-Schiffer and T. B. Rauchfuss, Hydrogenase Enzymes and Their Synthetic Models: The Role of Metal Hydrides, *Chem. Rev.*, 2016, **116**, 8693–8749.

10 G. A. N. Felton, C. A. Mebi, B. J. Petro, A. K. Vannucci, D. H. Evans, R. S. Glass and D. L. Lichtenberger, Review of electrochemical studies of complexes containing the Fe2S2 core characteristic of [FeFe]-hydrogenases including catalysis by these complexes of the reduction of acids to form dihydrogen, *J. Organomet. Chem.*, 2009, **694**, 2681–2699.

11 (*a*) H. Reihlen, A. Gruhl and G. V. Hessling, Über den photochemischen und oxydativen Abbau von Carbonylen, *Justus Liebigs Ann. Chem.*, 1929, **472**, 268–287; (*b*) W. Hieber and P. Spacu, Metal carbonyls. XXVI. Effect of organic sulfur compounds on the carbonyls of iron and cobalt, *Z. Anorg. Allg. Chem.*, 1937, **233**, 353–364; (*c*) J. A. Cabeza, M. A. Martínez-García, V. Riera, D. Ardura and S. García-Granda, Binuclear Iron(I), Ruthenium(I), and Osmium(I) Hexacarbonyl Complexes Containing a Bridging Benzene-1,2-dithiolate Ligand. Synthesis, X-ray Structures, Protonation Reactions, and EHMO Calculations, *Organometallics*, 1998, **17**, 1471–1477; (*d*) U.-P. Apfel, M. Rudolph, C. Apfel, C. Robl, D. Langenegger, D. Hoyer, B. Jaun, M.-O. Ebert, T. Alpermann, D. Seebach and W. Weigand, Reaction of $Fe_3(CO)_{12}$ with octreotide—chemical, electrochemical and biological investigations, *Dalton Trans.*, 2010, **39**, 3065–3071.

12 (*a*) J. L. Stanley, T. B. Rauchfuss and S. R. Wilson, Studies on the Condensation Pathway to and Properties of Diiron Azadithiolate Carbonyls, *Organometallics*, 2007, **26**, 1907–1911; (*b*) Y. Li and T. B. Rauchfuss, Synthesis of diiron(I) dithiolato carbonyl complexes, *Chem. Rev.*, 2016, **116**, 7043–7077; (*c*) L.-C. Song, Investigations on butterfly Fe/S cluster S-centered anions $(\mu\text{-S})_2Fe_2(CO)_6$, (μ-S)(μ-RS) $Fe_2(CO)_6$, and related species, *Acc. Chem. Res.*, 2005, **38**, 21–28; (*d*) L.-C. Song, F.-X. Luo, H. Tan, X.-J. Sun, Z.-J. Xie and H.-B. Song, Synthesis, structures, and properties of diiron azadithiolate complexes containing a subphthalocyanine moiety as biomimetic models for [FeFe]-hydrogenases, *Eur. J. Inorg. Chem.*, 2013, 2549–2557.

13 (*a*) I. Silaghi-Dumitrescu, T. E. Bitterwolf and R. B. King, Butterfly Diradical Intermediates in Photochemical Reactions of $Fe_2(CO)_6(\mu\text{-}S_2)$, *J. Am. Chem. Soc.*, 2006, **128**, 5342–5343; (*b*) A. Kramer and I. P. Lorenz, Photochemically induced [2 + 2] cycloadditions of alkenes and dienes with the sulfur-sulfur bond of the nido-clusters $[(O(C)_3Fe\ S]_2$, *J. Organomet. Chem.*, 1990, **388**, 187–193; (*c*) A. Kramer, R. Lingnau, I. P. Lorenz and H. L. Mayer, Complex-chemical synthesis of cyclic 1,2-dithiolato ligands with the nido cluster $[(CO)_3FeS]_2$. Molecular structure and partial S-oxidation of hexacarbonyl(μ_2-cis-1,2-cyclohexanedithiolato-S,S)diiron, *Chem. Ber.*, 1990, **123**, 1821–1826; (*d*) R. D. Adams and S. Miao, Metal Carbonyl Derivatives of Sulfur-Containing Quinones and Hydroquinones: Synthesis, Structures, and Electrochemical Properties, *Inorg. Chem.*, 2004, **43**, 8414–8426; (*e*) M. D. Westmeyer, T. B. Rauchfuss and A. K. Verma, Iron sulfido derivatives of the fullerenes C60 and C70, *Inorg. Chem.*, 1996, **35**, 7140–7147.

14 S. Aguado, L. Casarrubios, C. Ramírez de Arellano and M. A. Sierra, Revisiting the photochemical synthesis of [FeFe]-hydrogenase mimics: reaction optimization, mechanistic study and electrochemical behaviour, *RSC Adv.*, 2020, **10**, 29855–29867.

15 (*a*) M. Lian, J. He, X.-Y. Yu, C. Mu, X.-F. Liu, Y.-L. Li and Z.-Q. Jiang, Diiron ethanedithiolate complexes with acetate ester: Synthesis, characterization and electrochemical properties, *J. Organomet. Chem.*, 2018, **870**, 90–96; (*b*) S. Ghosh, S. Basak-Modi, M. G. Richmond, E. Nordlander and G. Hogarth, Electrocatalytic proton reduction by thiolate-capped triiron clusters $[Fe_3(CO)_9(\mu_3\text{-}SR)(\mu\text{-}H)]$ (R = iPr, tBu), *Inorg. Chim. Acta*, 2018, **480**, 47–53; (*c*) P.-H. Zhao, Z.-Y. Ma, M.-Y. Hu, J. He, Y.-Z. Wang, X.-B. Jing, H.-Y. Chen, Z. Wang and Y.-L. Li, PNP-Chelated and -Bridged Diiron Dithiolate Complexes Fe_2(μ-pdt)$(CO)_4\{(Ph_2P)_2NR\}$ Together with Related Monophosphine Complexes for the [2Fe]H Subsite of [FeFe]-Hydrogenases: Preparation, Structure, and Electrocatalysis, *Organometallics*, 2018, **37**, 1280–1290.

16 A. D. Merinero, A. Collado, L. Casarrubios, M. Gómez-Gallego, C. Ramírez de Arellano, A. Caballero, F. Zapata and M. A. Sierra, Triazole-Containing [FeFe] Hydrogenase Mimics: Synthesis and Electrocatalytic Behavior, *Inorg. Chem.*, 2019, **58**, 16267–16278.

17 A. Torres, D. J. Vicent, A. Collado, M. Gómez-Gallego, C. R. de Arellano and M. A. Sierra, Phosphite Bearing $[(\mu\text{-}ADT)^RFe_2(CO)_6]$ (ADT = Azadithiolate) Moieties: A Tool for the Building of Multimetallic [FeFe]-Hydrogenase Mimics, *Organometallics*, 2023, **42**, 316–326.

18 A. Torres, A. Collado, M. Gómez-Gallego, C. R. de Arellano and M. A. Sierra, Heteropolymetallic [FeFe]-Hydrogenase Mimics: Synthesis and Electrochemical Properties, *Inorg. Chem.*, 2023, **62**, 3409–3419.

19 J. D. Lawrence, H. Li and T. B. Rauchfuss, Beyond Fe-only hydrogenases: *N*-functionalized 2-aza-1,3-dithiolates $Fe_2[(SCH_2)_2NR](CO)_x$ (x = 5, 6), *Chem. Commun.*, 2001, 1482–1483.

20 X. Wang, G. Kehr, C. G. Daniliuc and G. Erker, Internal Adduct Formation of Active Intramolecular C4-bridged Frustrated Phosphane/Borane Lewis Pairs, *J. Am. Chem. Soc.*, 2014, **136**, 3293–3303.

21 J.-M. Heldt, N. Fischer-Durand, M. Salmain, A. Vessières and G. Jaouen, Preparation and characterization of poly(amido-amine) dendrimers functionalized with a rhenium carbonyl complex and PEG as new IR probes for carbonyl metallo immunoassay, *J. Organomet. Chem.*, 2004, **689**, 4775–4782.

22 M. L. Lage, I. Fernández, M. J. Mancheño, M. Gómez-Gallego and M. A. Sierra, The electronic structure and photochemistry of group 6 bimetallic (Fischer) carbene complexes: beyond the photocarbonylation reaction, *Chem. – Eur. J.*, 2010, **16**, 6616–6624.

23 (*a*) S. Ott, M. Kritikos, B. Åkermark and L. Sun, Synthesis and Structure of a Biomimetic Model of the Iron Hydrogenase Active Site Covalently Linked to a Ruthenium Photosensitizer, *Angew. Chem., Int. Ed.*, 2003, **42**, 3285–3288; (*b*) H. Wolpher, M. Borgström, L. Hammarström, J. Bergquist, V. Sundström, S. Styring, L. Sun and B. Åkermark, Synthesis and properties of an iron hydrogenase active site model linked to a ruthenium tris-bipyridine photosensitizer, *Inorg. Chem. Commun.*, 2003, **6**, 989–991; (*c*) S. Ott, M. Borgström, M. Kritikos, R. Lomoth, J. Bergquist, B. Åkermark, L. Hammarström and L. Sun, Model of the iron hydrogenase active site covalently linked to a ruthenium photosensitizer: synthesis and photophysical properties, *Inorg. Chem.*, 2004, **43**, 4683–4692; (*d*) J. Ekström, M. Abrahamsson, C. Olson, J. Bergquist, F. B. Kaynak, L. Eriksson, L. Sun, H.-C. Becker, B. Åkermark, L. Hammarström and S. Ott, Bio-inspired, side-on attachment of a ruthenium photosensitizer to an iron hydrogenase active site model, *Dalton Trans.*, 2006, 4599–4606; (*e*) W. Gao, J. Liu, W. Jiang, M. Wang, L. Weng, B. Åkermark and L. Sun, An azadithiolate bridged Fe_2S_2 complex as active site model of FeFe-hydrogenase covalently linked to a $Re(CO)_3(bpy)(py)$ photosensitizer aiming for light-driven hydrogen production, *C. R. Chim.*, 2008, **11**, 915–921.

24 R. Lomoth and S. Ott, Introducing a dark reaction to photochemistry: photocatalytic hydrogen from [FeFe] hydrogenase active site model complexes, *Dalton Trans.*, 2009, **45**, 9952–9959.

25 P. Poddutoori, D. T. Co, A. P. S. Samuel, C. H. Kim, M. T. Vagnini and M. R. Wasielewski, Photoinitiated multistep charge separation in ferrocene–zinc porphyrin–diiron hydrogenase model complex triads, *Energy Environ. Sci.*, 2011, **4**, 2441–2450.

26 H. Mizuno, J. Takaya and N. Iwasawa, Rhodium(I)-Catalyzed Direct Carboxylation of Arenes with CO2 via Chelation-Assisted C−H Bond Activation, *J. Am. Chem. Soc.*, 2011, **133**, 1251–1253.

27 J. Hu, M. Gao, Y. Zhang, Y. Wang, Z. Qiao, W. Zhang, Q. Wang, L. Yan and H. Qian, Novel piperazine urea derivatives as highly potent transient receptor potential vanilloid 1 (TRPV1) antagonists, *Bioorg. Chem.*, 2021, **115**, 105229.

28 T. Mochida, H. Shimizu, S. Suzuki and T. Akasaka, Synthesis and properties of azole-substituted ferrocenes, *J. Organomet. Chem.*, 2006, **691**, 4882–4889.

29 (*a*) F. Wang, M. Wang, X. Liu, K. Jin, W. Dong and L. Sun, Protonation, electrochemical properties and molecular structures of halogen-functionalized diiron azadithiolate complexes related to the active site of iron-only hydrogenases, *Dalton Trans.*, 2007, **34**, 3812–3819; (*b*) G. Eilers, L. Schwartz, M. Stein, G. Zampella, L. de Gioia, S. Ott and R. Lomoth, Ligand versus Metal Protonation of an Iron Hydrogenase Active Site Mimic, *Chem. – Eur. J.*, 2007, **13**, 7075–7084; (*c*) L. Schwartz, G. Eilers, L. Eriksson, A. Gogoll, R. Lomoth and S. Ott, Iron hydrogenase active site mimic holding a proton and a hydride, *Chem. Commun.*, 2006, **5**, 520–522.

30 M. Watanabe, Y. Honda, H. Hagiwara and T. Ishihara, [FeFe]-Hydrogenase and its organic molecule mimics—Artificial and bioengineering application for hydrogenproduction, *J. Photochem. Photobiol., C*, 2017, **33**, 1–26.

31 W.-G. Wang, H.-Y. Wang, G. Si, C.-H. Tung and L.-Z. Wu, Fluorophenyl-substituted Fe-only hydrogenases active site ADT models: different electrocatalytic process for proton reduction in HOAc and HBF_4/Et_2O, *Dalton Trans.*, 2009, **15**, 2712–2720.

32 G. A. Felton, R. S. Glass, D. L. Lichtenberger and D. H. Evans, Iron-only hydrogenase mimics. Thermodynamic aspects of the use of electrochemistry to evaluate catalytic efficiency for hydrogen generation, *Inorg. Chem.*, 2006, **45**, 9181–9184.

33 S. Gao, Q. Liang, Q. Duan, D. Jiang and J. Zhao, Electrochemical proton reductions in varying acidic media by a simple synthetic hydrogenase mimic, *Int. J. Hydrogen Energy*, 2018, **43**, 7245–7256.

34 M. P. Stewart, M.-H. Ho, S. Wiese, M. L. Lindstrom, C. E. Thogerson, S. Raugei, R. M. Bullock and M. L. Helm, High Catalytic Rates for Hydrogen Production Using Nickel Electrocatalysts with Seven-Membered Cyclic Diphosphine Ligands Containing One Pendant Amine, *J. Am. Chem. Soc.*, 2013, **135**, 6033–6046.

35 H.-M. Cui, M.-Q. Hu, H.-M. Wen, G.-L. Chai, C.-B. Ma, H. Chen and C.-N. Chen, Efficient [FeFe] hydrogenase mimic dyads covalently linking to iridium photosensitizer for photocatalytic hydrogen evolution, *Dalton Trans.*, 2012, **41**, 13899–13907.

